Arnaud Malher
IMSIA (Institute of Mechanical Sciences and
Industrial Applications),
ENSTA ParisTech—CNRS—EDF—CEA,
Université Paris-Saclay,
828 Bd des Maréchaux,
Palaiseau Cedex 91732, France
e-mails: arnaud.malher@ensta-paristech.fr,
arnaud.malher@gmail.com

Cyril Touzé
IMSIA (Institute of Mechanical Sciences
and Industrial Applications),
ENSTA ParisTech—CNRS—EDF—CEA,
Université Paris-Saclay,
828 Bd des Maréchaux,
Palaiseau Cedex 91732, France

Olivier Doaré
IMSIA (Institute of Mechanical Sciences and
Industrial Applications),
ENSTA ParisTech—CNRS—EDF—CEA,
Université Paris-Saclay,
828 Bd des Maréchaux,
Palaiseau Cedex 91732, France

Giuseppe Habib
Space Structures and Systems Laboratory,
Department of Aerospace and
Mechanical Engineering,
University of Liège,
Liège 4000, Belgium

Gaëtan Kerschen
Space Structures and Systems Laboratory,
Department of Aerospace and
Mechanical Engineering,
University of Liège,
Liège 4000, Belgium

Flutter Control of a Two-Degrees-of-Freedom Airfoil Using a Nonlinear Tuned Vibration Absorber

The influence of a nonlinear tuned vibration absorber (NLTVA) on the airfoil flutter is investigated. In particular, its effect on the instability threshold and the potential subcriticality of the bifurcation is analyzed. For that purpose, the airfoil is modeled using the classical pitch and plunge aeroelastic model together with a linear approach for the aerodynamic loads. Large amplitude motions of the airfoil are taken into account with nonlinear restoring forces for the pitch and plunge degrees-of-freedom. The two cases of a hardening and a softening spring behavior are investigated. The influence of each NLTVA parameter is studied, and an optimum tuning of these parameters is found. The study reveals the ability of the NLTVA to shift the instability, avoid its possible subcriticality, and reduce the limit cycle oscillations (LCOs) amplitude. [DOI: 10.1115/1.4036420]

Keywords: flutter instability, nonlinear tuned vibration absorber, tuned mass damper, passive control

1 Introduction

When slender structures, such as bridge deck or airfoil, undergo wind excitation, a flutter instability, triggered by a Hopf bifurcation, may arise. The flow velocity for which the instability starts is called the *flutter velocity*. This phenomenon is detrimental and may even lead to fatal vibrations of the structure.

Numerous strategies have been investigated in the past in order to control the flutter instability. Most of them concern active control techniques, such as governing a trailing edge flap on the wing [1–3] or using piezoelectric actuators [4]. The reader may refer to the Dowell's book on aeroelasticity [5] for more details on flutter active control. The alternative strategy is the use of passive control techniques [6], which is also the aim of the present study. This research topic is relatively recent. Most efforts have been devoted to bridge deck passive control [7–9].

The most classical passive device for controlling flutter instabilities is the tuned vibration absorber (TVA) initially developed by Den Hartog [10], and generally known as tuned mass damper (TMD) or TVA. This device consists of a small-lumped mass attached to the primary structure through a linear spring and a damper. If its

eigenfrequency and damping ratio are correctly tuned, it can significantly shift the flutter speed [11]. Nevertheless, the TMD has no effect on the nonlinearities arising in the post-critical regime.

Lee et al. [12,13] proposed to use a nonlinear energy sink (NES) to control the flutter instability. The NES has been initially investigated in the field of vibration control [14–16], it consists of an oscillator linked to the primary structure through an essential nonlinear stiffness (i.e., with no linear part), leading to targeted energy transfer [17]. Applied to the flutter control, the method shows an important reduction in the amplitude of the LCOs [12,13,18,19]. Nevertheless, it has no effect on the flutter velocity and needs a certain amount of energy to be activated.

In the present study, the use of a NLTVA, as proposed by Viguié and Kerschen [20] and Habib et al. [21], is investigated. The distinctive feature of the NLTVA is that it possesses both a linear and a nonlinear stiffness. The linear part of the absorber enables to recover the optimal control given by a TMD, whereas its nonlinear part can be tuned in order to enhance the control of the primary system nonlinearities, using a so-called principle of similarity [22]. Its effectiveness has been proven on a Van der Pol-Duffing oscillator [23]. Moreover, several experimental realizations of the NLTVA have been recently explored [24,25], and a tuning rule for the NLTVA parameters coupled with a primary system having polynomial nonlinearities has been proposed using the Den Hartog's equal peak method [22].

In the present context of the flutter instability, two main design rules are followed for optimizing the NLTVA characteristics. First, the linear stiffness of the absorber is tuned in order to increase as much as possible the critical flutter velocity, thus repelling the appearance of LCO to larger flow velocities. This step consists of finding the optimal values of a TMD in order to control the flutter instability, for which the preliminary results can be found in Ref. [26] for a specific set of airfoil parameters. Second, the nonlinear stiffness of the NLTVA may be tuned in order to enforce supercriticality, as well as to reduce the LCO amplitudes. The aim of the present study is thus to extend the results presented in Ref. [23], obtained for a Van der Pol-Duffing oscillator as a primary structure. To get closer to a real airfoil situation, the primary structure is selected here as the classical two degrees-of-freedom aeroelastic system, with pitch and plunge motions as generalized coordinates [5]. The quasi-steady theory is used to estimate the aerodynamic loads. In order to take into account the nonlinear structural behavior for large displacements, the model includes cubic stiffness terms in the pitch and plunge motion. This allows the system to develop LCO in the post-critical regime.

The first section is devoted to the linear stability analysis. The optimization of the linear characteristics of the vibration absorber is investigated, showing in particular how the flutter velocity can be repelled to larger values using a well-tuned absorber. The airfoil parameters are then varied, and a design rule is proposed in order to find easily the optimized linear values. Then, the influence of the nonlinear part of the NLTVA is investigated. Two different cases are specifically studied for the airfoil nonlinear restoring force: a hardening and a softening scenario. These results give a number of fruitful strategies in order to control passively the flutter instability by means of a nonlinear vibration absorber.

2 Equations of Motion

2.1 Model Equations. The classical pitch and plunge model is used to describe the airfoil motion, see, e.g., Ref. [5]. Pitch and plunge are, respectively, described by the heave h and the angle of attack α as shown in Fig. 1. The geometrical parameters of the airfoil are the chord c, the semichord b, and the lifting surface S. EC is the elastic center, GC the gravity center, and AC the aerodynamic center. The distance between AC and EC is denoted by e. The inertia terms of the airfoil are the mass M, the inertia moment I_α, and the static moment S_α. The static moment S_α is equal to Mx_{CG}, where x_{CG} is the distance between EC and GC. The pitch mode is described by the stiffness k_α and the damping c_α and the plunge motion by the stiffness k_h and the damping c_h. The model encompasses structural nonlinearities, which have the beneficial effect of limiting the dynamics to LCOs in the post-critical regime. Nonlinear terms in the plunge and pitch stiffnesses, respectively, k_{h3} and $k_{\alpha3}$, are thus introduced in a similar fashion as in Refs. [12], [13], [27], and [28] in order to take into account the potential nonlinearities of the aeroelastic system that can arise from, e.g., geometric or localized nonlinearities.

The flow goes from left to right with velocity U, as illustrated in Fig. 1. It produces two aerodynamic loads, the lift L and the aerodynamic moment M_a. The quasi-steady theory is selected for modeling them, see, e.g., Refs. [5] and [29]. It gives the following expressions: $L = (1/2)\rho\,S\,U^2 \mathrm{d}C_l(\alpha + \dot{h}/U)$ and $M_a = (1/2)\rho\,S\,c\,U^2\,e\,\mathrm{d}C_l(\alpha + \dot{h}/U)$, where ρ is the fluid density, and $\mathrm{d}C_l$ is the slope at zero angle of attack of the lift coefficient.

The NLTVA is attached along the midchord of the airfoil at distance l from EC. It is composed of a mass m, a spring of linear stiffness k and cubic stiffness k_3, and a dashpot of damping c. Finally, the equations of motion read

$$M\ddot{h} + S_\alpha\ddot{\alpha} + (c_h + BU)\dot{h} + c(\dot{h} - \dot{x} - l\dot{\alpha})$$
$$+ k_h h + BU^2\alpha + k(h - x - l\alpha)$$
$$+ k_{h3}\,h^3 + k_3(h - x - l\alpha)^3 = 0 \qquad (1a)$$

$$I_\alpha\ddot{\alpha} + S_\alpha\ddot{h} + c_\alpha\dot{\alpha} + c\,l(\dot{x} + l\dot{\alpha} - \dot{h}) - NU\dot{h}$$
$$+ (k_\alpha - NU^2)\alpha + k\,l(x + l\alpha - h)$$
$$+ k_{\alpha3}\,\alpha^3 + k_3\,l(x + l\alpha - h)^3 = 0 \qquad (1b)$$

$$m\ddot{x} + c(\dot{x} + l\dot{\alpha} - \dot{h}) + k(x + l\alpha - h) + k_3(x + l\alpha - h)^3 = 0 \quad (1c)$$

where $B = (1/2)\,\rho S\,\mathrm{d}C_l$, and $N = (1/2)\,\rho S\,e\,\mathrm{d}C_l$.

The aim of the linear part of the NLTVA, which can be seen as a TMD, is to repel the flutter velocity. The goal of its nonlinear part is to reduce the LCO amplitude and ensure the supercriticality of the bifurcation caused by the flutter instability. The NLTVA nonlinear part is limited to a cubic stiffness in order to have the same functional form as the airfoil nonlinearity as prescribed in Ref. [23].

In order to reduce the number of the system parameters, the equations of motion are made dimensionless, by introducing

$$y = h/b \quad \text{and} \quad \tilde{x} = x/b$$

The inertia coefficients become

$$r_\alpha = \sqrt{I_\alpha/Mb^2} \quad \text{and} \quad x_\alpha = S_\alpha/Mb$$

Afterward, by introducing the dimensionless time $\tau = \omega_\alpha t$, where $\omega_\alpha = \sqrt{k_\alpha/I_\alpha}$, the expression of the frequency ratio, dimensionless cubic stiffnesses, and damping ratios are obtained as

$$\omega_h = \sqrt{k_h/M}, \ \Omega = \omega_h/\omega_\alpha, \ \xi_h = k_{h3}/(M\,\omega_\alpha^2),$$
$$\xi_\alpha = k_{\alpha3}/(M\,b^2\,\omega_\alpha^2), \ \zeta_h = c_h/M\omega_\alpha \text{ and } \zeta = c/m\omega_\alpha$$

Then, the dimensionless aerodynamic parameters are introduced as follows:

$$\tilde{U} = U/b\omega_\alpha, \ \beta = B\,b/M \text{ and } \nu = N/M$$

Eventually, the dimensionless NLTVA parameters are

$$\varepsilon = m/M, \ \omega = \sqrt{k/m}, \ \gamma = \omega^2/\omega_\alpha^2, \ \lambda = l/b,$$
$$\zeta = c/m\omega_\alpha, \text{ and } \xi = k_3/(m\,\omega_\alpha^2)$$

The equations of motion finally can be recast in compact form as

$$\mathbf{M}\mathbf{q}'' + \mathbf{C}\mathbf{q}' + \mathbf{K}\mathbf{q} + \mathbf{F}(\mathbf{q}) = 0 \qquad (2)$$

with

$$\mathbf{q} = \begin{bmatrix} y \\ \alpha \\ \tilde{x} \end{bmatrix}, \quad \mathbf{M} = \begin{bmatrix} 1 & x_\alpha & 0 \\ x_\alpha & r_\alpha^2 & 0 \\ 0 & 0 & 1 \end{bmatrix},$$
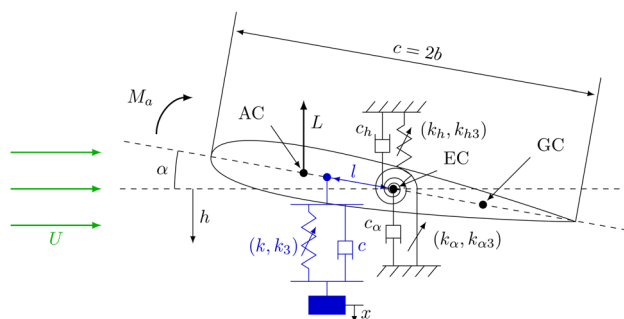

Fig. 1 Sketch of the two degrees-of-freedom airfoil (main structure) coupled with the NLTVA (absorber)

$$\mathbf{C} = \begin{bmatrix} \zeta_h + \epsilon\zeta + \beta\tilde{U} & -\epsilon\zeta\lambda & -\epsilon\zeta \\ -\nu\tilde{U} - \epsilon\zeta\lambda & \zeta_\alpha + \epsilon\zeta\lambda^2 & \epsilon\zeta\lambda \\ -\zeta & \zeta\lambda & \zeta \end{bmatrix}$$

$$\mathbf{K} = \begin{bmatrix} \Omega^2 + \epsilon\gamma & \beta\tilde{U}^2 - \epsilon\gamma\lambda & -\epsilon\gamma \\ -\epsilon\gamma\lambda & r_\alpha^2 - \nu\tilde{U}^2 + \epsilon\gamma\lambda^2 & \epsilon\gamma\lambda \\ -\gamma & \gamma\lambda & \gamma \end{bmatrix}$$

and

$$\mathbf{F}(\mathbf{q}) = \begin{bmatrix} \xi_h y^3 + \epsilon\,\xi(y - \tilde{x} - \lambda\alpha)^3 \\ \xi_\alpha \alpha^3 + \epsilon\lambda\,\xi(\tilde{x} + \lambda\alpha - y)^3 \\ \xi(\tilde{x} + \lambda\alpha - y)^3 \end{bmatrix}$$

where $(\ )' = d/d\tau$.

The characteristics of the NLTVA are defined according the following five parameters:

(1) the mass ratio $\epsilon = m/M$, between the mass of the NLTVA and that of the wing;
(2) the dimensionless distance λ that specifies the location where the NLTVA is attached;
(3) the NLTVA-reduced eigenfrequency $\gamma = \omega^2/\omega_\alpha^2$, characterizing the eigenfrequency of the NLTVA compared to that of pitch motion;
(4) the NLTVA damping ratio $\zeta = c/m\omega_\alpha$; and
(5) the NLTVA-reduced cubic stiffness $\xi = k_3/(m\,\omega_\alpha^2)$.

For the present study, the mass ratio has been taken equal to 5%. The larger the ϵ the more efficient the NLTVA will be, however, one must keep in mind that the absorber needs to have a negligible mass as compared to the airfoil. In this work, the NLTVA is located at the leading edge of the profile, thus, $\lambda = 1$. Note that its effect has been found, in our study, to be directly proportional to λ. Hence, the location where its influence on the airfoil is optimal has been selected. Eventually, γ and ζ are thus selected as our linear control parameters and ξ as our nonlinear control parameter, the optimal tuning of which is searched for.

2.2 Flutter Velocity. The aim of this section is to introduce the flutter velocity of the airfoil system alone, which will be afterward compared to that obtained with the presence of the absorber. The linear part of the equations of motion without the NLTVA writes

$$\begin{bmatrix} 1 & x_\alpha \\ x_\alpha & r_\alpha^2 \end{bmatrix}\begin{bmatrix} y'' \\ \alpha'' \end{bmatrix} + \begin{bmatrix} \zeta_h + \beta\tilde{U} & 0 \\ -\nu\tilde{U} & \zeta_\alpha \end{bmatrix}\begin{bmatrix} y' \\ \alpha' \end{bmatrix}$$
$$+ \begin{bmatrix} \Omega^2 & \beta\tilde{U}^2 \\ 0 & r_\alpha^2 - \nu\tilde{U}^2 \end{bmatrix}\begin{bmatrix} y \\ \alpha \end{bmatrix} = 0 \tag{3}$$

Table 1 Dimensionless aeroelastic parameters of the reference case [5]

x_α	r_α	β	ν	Ω	ζ_α	ζ_h
0.2	0.5	0.2	0.08	0.5	0.01	0.01

We assume a solution of the form

$$\begin{bmatrix} y \\ \alpha \end{bmatrix} = \begin{bmatrix} y_0 \\ \alpha_0 \end{bmatrix} \exp(z\,t) \tag{4}$$

where $y_0 = y(0)$, $\alpha_0 = \alpha(0)$, and $z \in \mathbb{C}$. Therefore, three situations are possible:

(1) $\Re(z) < 0$, the airfoil motion is stable;
(2) $\Re(z) \geq 0$ and $\Im(z) \neq 0$, the airfoil encounters flutter; and
(3) $\Re(z) \geq 0$ and $\Im(z) = 0$, the airfoil encounters divergence.

The linear system Eq. (3) with the ansatz (4) writes

$$\mathbf{B}\begin{bmatrix} y_0 \\ \alpha_0 \end{bmatrix}\exp(z\,t) = 0 \quad \text{with}$$

$$\mathbf{B} = \begin{bmatrix} z^2 + \zeta_h z + \beta\tilde{U}z + \Omega^2 & x_\alpha z^2 + \beta\tilde{U}^2 \\ x_\alpha z^2 - \nu\tilde{U}z & r_\alpha^2 z^2 + \zeta_\alpha z + r_\alpha^2 - \nu\tilde{U}^2 \end{bmatrix}$$

By canceling the determinant of $\mathbf{B}$, the flutter velocity $\tilde{U}_f$ can be found, as shown in Refs. [5], [6], and [29–31].

Section 3 is devoted to the linear stability analysis in the presence of the NLTVA. The calculation will follow the same guidelines recalled here.

3 Linear Stability Analysis

3.1 Optimization of the NLTVA Linear Parameters. The aim of this section is to study the influence of the design parameters γ and ζ on the flutter velocity $\tilde{U}_f$. The targeted optimal values are those for which $\tilde{U}_f$ is as large as possible, in order to repel the instability.

In the remaining of this study, unless explicitly mentioned, the airfoil linear parameters of Eq. (2) are equal to the parameters from Ref. [5]. They are gathered in Table 1 and define the reference case. In the next section, the airfoil parameters will be varied in order to investigate their influence on the NLTVA tuning and effectiveness. In Sec. 3, the nonlinear terms are not taken into account.

Using the same notations as Sec. 2.2, $\mathbf{B}$ is now equal to

$$\mathbf{B} = \begin{bmatrix} z^2 + (\zeta_h + \epsilon\zeta + \beta\tilde{U})z + \Omega^2 + \epsilon\gamma & x_\alpha z^2 - \epsilon\zeta\lambda z + \beta\tilde{U}^2 - \epsilon\gamma\lambda & -\epsilon\zeta z - \epsilon\gamma \\ x_\alpha z^2 - (\nu\tilde{U} - \epsilon\zeta\lambda)z - \epsilon\gamma\lambda & r_\alpha^2 z^2 + (\zeta_\alpha + \epsilon\zeta\lambda^2)z + r_\alpha^2 - \nu\tilde{U}^2 + \epsilon\gamma\lambda^2 & \epsilon\zeta\lambda z + \epsilon\gamma\lambda \\ -\zeta z - \gamma & \zeta\lambda z + \gamma\lambda & z^2 + \zeta z + \gamma \end{bmatrix}$$

The determinant of the matrix $\mathbf{B}$ takes the form of a sixth-order polynomial

$$\det(\mathbf{B}) = a_6 z^6 + a_5 z^5 + a_4 z^4 + a_3 z^3 + a_2 z^2 + a_1 z + a_0 \tag{5}$$

where $a_1 – a_6$ are detailed in Appendix A. The Routh–Hurwitz criterion is used to determine when one of the roots of $\det(\mathbf{B})$ has a positive real part.

This study leads to four independent conditions called b_5, c_5, d_5, and e_5, which read $b_5 = (a_5 a_4 - a_6 a_3)/a_5 > 0$, $c_5 = b_5 a_3 - a_5 b_4 > 0$, $d_5 = c_5 b_4 - c_4 b_5 > 0$, and $e_5 = d_5 c_4 - d_4 c_5 > 0$, with $b_4 = (a_5 a_2 - a_6 a_1)/a_5$, $b_3 = a_0$, $c_4 = (b_5 a_3 - b_3 a_5)/b_5$ and $d_4 = b3$.

These four conditions are plotted as an example in Fig. 2 for $\zeta = 0.15$. Each line corresponds to the points where one of the four expressions b_5–e_5 becomes positive, as a function of the reduced eigenfrequency γ, and for increasing values of $\tilde{U}$. Thus, the flutter velocity corresponds to the lowest curve and the stability zone to the area below it, represented as a gray-shaded area in Fig. 2.

This calculation is then conducted for different values of ζ in order to find the optimal couple $(\gamma_{\text{opt}}, \zeta_{\text{opt}})$ for which the flutter velocity is maximal. The result is shown in Fig. 3. The maximal reduced flutter velocity, obtained for $\gamma = 0.462$ and $\zeta = 0.11$, is equal to 1.255, which means a 34.5% gain as compared to the flutter velocity without the absorber, which is equal to 0.934. This gain on the flutter velocity is named $G_{\tilde{U}_f}$ and is equal to

$$G_{\tilde{U}_f} = \frac{\tilde{U}_f^{\text{NLTVA}} - \tilde{U}_f^{\text{noTVA}}}{\tilde{U}_f^{\text{noTVA}}}$$

where $\tilde{U}_f^{\text{noTVA}}$ is the flutter speed of the system without absorber and $\tilde{U}_f^{\text{NLTVA}}$ with the NLTVA. Because of their complexity, the equations $b_5 = 0$, $c_5 = 0$, $d_5 = 0$, and $e_5 = 0$ cannot be easily made explicit with respect to ζ and γ. Thus, analytical expressions of the optimal values of ζ and γ are not defined. Nevertheless, these optimal values can be found numerically.

In practical situations, a slight detuning of γ and ζ may occur. Thus, the sensitivity of $\tilde{U}_f$ regarding these parameters is detailed. It is shown in Fig. 3 that γ has more influence on $\tilde{U}_f$ than ζ. Moreover, $\tilde{U}_f^{\text{max}}$ is on a sharp point rather than on a plateau. That is, if γ increases a little, $\tilde{U}_f$ decreases significantly. Nevertheless, if γ decreases a little, the $\tilde{U}_f$'s drop is less abrupt. Therefore, the control should guarantee $\gamma \leq \gamma_{\text{opt}}$. For a more quantitative point of view, a 10% increase of γ gives a 20% decrease of $\tilde{U}_f$ and a 10% decrease of γ implies a 7% decrease of $\tilde{U}_f$, whereas a 10% increase or decrease of ζ gives a 4% decrease of $\tilde{U}_f$.

3.2 Influence of the Airfoil Parameters. In this section, the airfoil parameters' influence on the NLTVA efficiency is investigated. Three main parameters are identified for characterizing the airfoil: the nondimensional static moment $x_\alpha = S_\alpha/(Mb)$, which describes the coupling between pitch and plunge motion, the radius of gyration $r_\alpha = \sqrt{I_\alpha/(M b^2)}$, which expresses the ratio
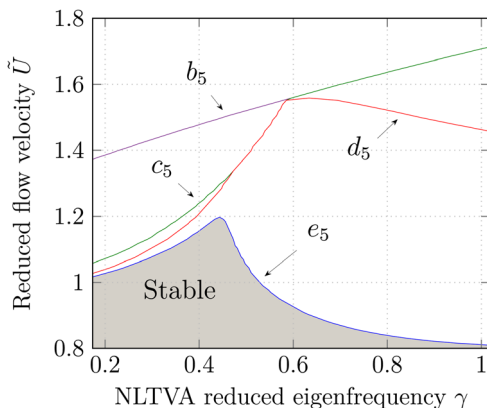
between the airfoil inertias, and finally, the frequency ratio $\Omega = \omega_h/\omega_\alpha$ between the two natural frequencies of the plunge and pitch motion.
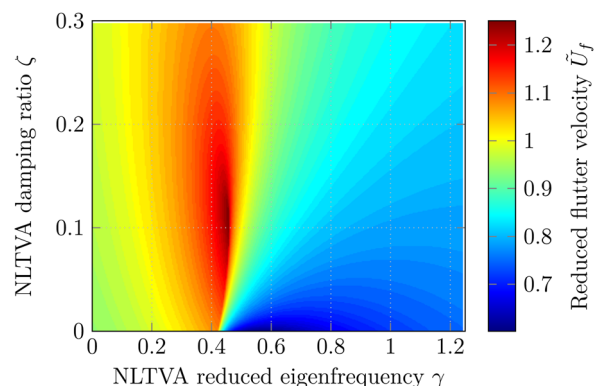
Let us now define the investigation range for each of these three selected parameters.

The location of EC from the leading edge is equal to 0.45 c in the reference case. The selected investigation range is selected as [0 0.6]. The extreme value for x_α is $x_\alpha = 1.1$; corresponding to a gravity center at the trailing edge, however, this situation never occurs in practice. The value for r_α^2 depends on the airfoil density distribution and shape. Although theoretically not bounded, it is generally in the interval [0 1] [29,32,33]; which is thus the selected range in this study. Finally, variations of Ω^2 are selected in the range [0 1]. Indeed, the natural frequency of the pitch motion is generally larger than the plunge one, thus, $\Omega^2 \leq 1$.

The optimal value γ_{opt} and ζ_{opt} are computed using the methodology described in Sec. 3.1, while varying the three parameters x_α, r_α^2, and Ω^2 in their respective ranges. The corresponding gain in flutter velocity, $G_{\tilde{U}_f}$, is plotted in Fig. 4. The color represents the value of $G_{\tilde{U}_f}$ for each set of airfoil parameters. The influence of the NLTVA on $G_{\tilde{U}_f}$ is highly dependent on the airfoil parameters and can vary from 10% up to more than 140%.

General tendencies on the influence of x_α, r_α^2, and Ω^2 on the flutter velocity gain $G_{\tilde{U}_f}$ can be drawn from Fig. 4. First of all, there is a small strip of large $G_{\tilde{U}_f}$ for small values of r_α^2, especially visible for $\Omega^2 = 0.4$ and 0.7. This small strip has a singular behavior, but the corresponding value of r_α^2 are particularly small and not very realistic. Otherwise, the influence of r_α^2 is limited. Regarding Ω^2, the larger it is the larger is $G_{\tilde{U}_f}$. Indeed, when Ω^2 is close to one, ω_α and ω_h are close to each other. In this case, the efficiency of the NLTVA, working optimally at a single frequency, is enhanced since both degrees-of-freedom can be controlled. Eventually, the influence of x_α is substantial, the NLTVA effectiveness decreasing while x_α is increasing. The explanation of this tendency is not obvious. An argument that can be given is that a large x_α push the two airfoil-coupled frequencies apart. Thus, as for Ω^2, the same causes producing the same effects, if x_α is large the NLTVA is less efficient.

3.3 NLTVA Linear Parameters Tuning Rule. The aim of the present section is to provide a simple tuning rule allowing one to compute easily the optimal NLTVA linear parameters, namely, γ_{opt} and ζ_{opt}; as a function of the airfoil parameters, condensed in the three-dimensionless parameters x_α, r_α^2, and Ω^2. For that purpose, a third-order polynomial expansion has been found to give an accurate fit to the hypersurface shown in Fig. 4. More specifically, the following expansion has been used:

Fig. 2 Reduced flutter velocity given by the Routh–Hurwitz criterion as a function of the NLTVA-reduced eigenfrequency γ, and for a damping ratio $\zeta = 0.15$. The gray area corresponds to the stability of the system.

Fig. 3 Cartography of the reduced flutter velocity given by the criterion e_5 as a function of the NLTVA-reduced frequency γ and damping ratio ζ
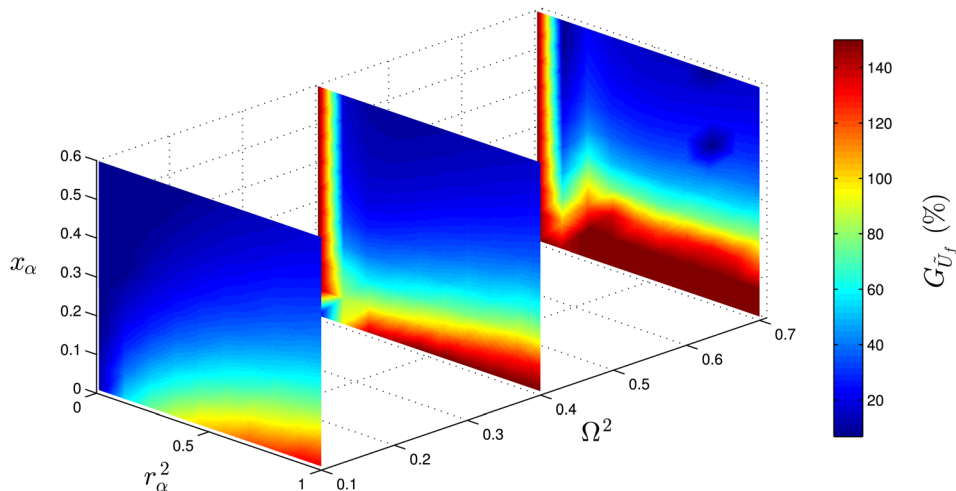
Fig. 4 Evolution of the optimal flutter velocity gain $G_{\tilde{U}_f}$ caused by the NLTVA versus x_α, r_α^2, and Ω^2

$$\gamma_{\text{opt}}^{\text{fit}} = \sum_{i,j,k=0}^{3} a_{ijk}\, x_\alpha^i \left(r_\alpha^2\right)^j \left(\Omega^2\right)^k$$

$$\zeta_{\text{opt}}^{\text{fit}} = \sum_{i,j,k=0}^{3} b_{ijk}\, x_\alpha^i \left(r_\alpha^2\right)^j \left(\Omega^2\right)^k \qquad (6)$$

the coefficients of which are given in Appendix B. The resulting $G_{\tilde{U}_f}$, calculated with $\gamma_{\text{opt}}^{\text{fit}}$ and $\zeta_{\text{opt}}^{\text{fit}}$, is plotted in Fig. 5. This figure has to be compared with Fig. 4, showing that the qualitative and quantitative features are retrieved. Hence, Eq. (6) can be easily used in order to determine directly the NLTVA linear parameters as a function of its airfoil parameters.

4 Nonlinear Analysis of the Post-Critical Regime

This section is devoted to the tuning methodology for optimizing the nonlinear stiffness of the NLTVA. Two goals are in view. First, one would like to ensure a supercritical bifurcation, as being a safer scenario for an engineering design with respect to the global stability of the airfoil. Second, the post-critical LCOs are investigated in order to decrease their amplitudes as much as possible.

For the nonlinear analysis, the NLTVA linear parameters correspond to the airfoil reference case and are gathered in Table 2.

4.1 Criticality Analysis. The Hopf bifurcation encountered at $\tilde{U} = \tilde{U}_f$ can be either subcritical or supercritical. In a normal form analysis of the bifurcation, this characteristic is simply related to the sign of the cubic nonlinear term when the system is written in polar form [34–36]. The aim of this section is to obtain the expression of this coefficient, based on a reduced-order model that contains the leading-order nonlinearity of the normal form. The technique used follows classical methods for dynamical systems [34,37] that have been recently applied on a Van der Pol-Duffing oscillator [23]. It is decomposed into five steps.

The first step is to recast the equations of motion (2) as a first-order dynamical system as follows:

$$\tilde{\mathbf{q}}' = A\tilde{q} + \mathbf{b} \qquad (7)$$

with

$$\tilde{\mathbf{q}} = \begin{bmatrix} y \\ \alpha \\ \tilde{x} \\ y' \\ \alpha' \\ \tilde{x}' \end{bmatrix}, \quad \mathbf{A} = \begin{bmatrix} 0_3 & Id_3 \\ -\mathbf{M}^{-1}\mathbf{K} & -\mathbf{M}^{-1}\mathbf{C} \end{bmatrix},$$
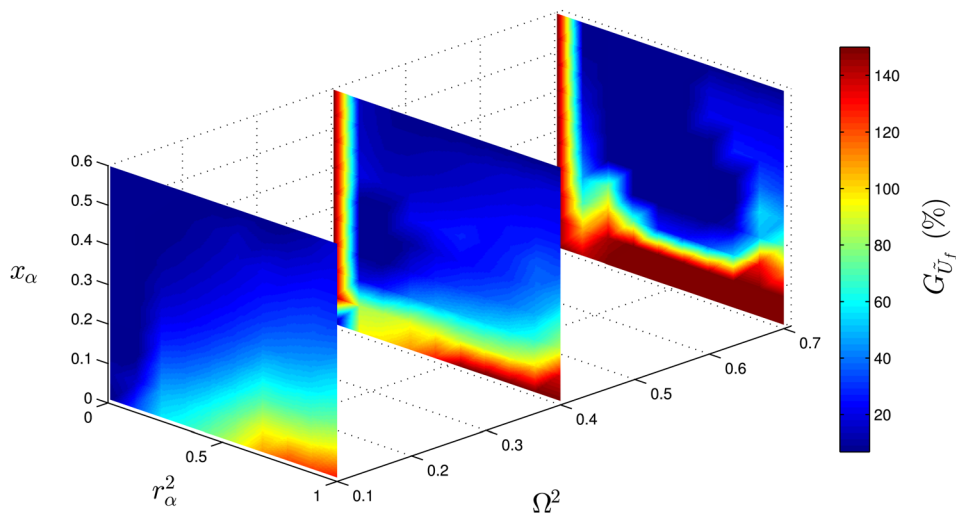
Fig. 5 Estimation of $G_{\tilde{U}_f}$ using the fitted parameters $\zeta_{\text{opt}}^{\text{fit}}$ and $\gamma_{\text{opt}}^{\text{fit}}$ versus x_α, r_α^2 and Ω^2

Table 2   NLTVA linear parameters used for the nonlinear analysis

ε	λ	ζ	γ
0.05	1	0.11	0.462

$$\mathbf{b} = \begin{bmatrix} 0 \\ 0 \\ 0 \\ -\mathbf{M}^{-1} \begin{bmatrix} \xi_h y^3 + \varepsilon\xi(y - \tilde{x} - \lambda\alpha)^3 \\ \xi_\alpha \alpha^3 + \varepsilon\xi\lambda(\tilde{x} - y + \lambda\alpha)^3 \\ \xi(\tilde{x} - y + \lambda\alpha)^3 \end{bmatrix} \end{bmatrix}$$

For the criticality analysis, ξ_α, ξ_h, and ξ are left variable, ξ being the nonlinear control parameter of the NLTVA.

The second step is to estimate the eigenvalues and eigenvectors of $\mathbf{A}$ for $\tilde{U} = \tilde{U}_f$. Because the expression of $\mathbf{A}$ is particularly tedious, an analytical expression of its eigenvectors and eigenvalues is not reachable, and they are thus calculated using the airfoil parameters from Table 1 and the retained NLTVA linear parameters. The system being of dimension 6, the eigenvalues and eigenvectors of $\mathbf{A}$ for $\tilde{U} = \tilde{U}_f$ are denoted, respectively, as d_1–d_6 and $\mathbf{V}_1$–$\mathbf{V}_6$. Besides, the real and imaginary part of $d_{1...6}$ are denoted as $\lambda_{1...6}$ and $\omega_{1...6}$, respectively. The Hopf bifurcation is characterized by a pair of complex conjugate eigenvalues crossing the imaginary axis. At criticality for $\tilde{U} = \tilde{U}_f$, these eigenvalues, denoted d_1 and d_2, have a zero real part and read

$$d_1 = i\,\omega_1 \quad \text{and} \quad d_2 = i\,\omega_2 = -i\,\omega_1$$

Their corresponding eigenvectors are denoted $\mathbf{V}_1$ and $\mathbf{V}_2$. Because it has been found that in our case $\mathbf{V}_1$–$\mathbf{V}_6$ are complex conjugates, and the following transformation matrix is introduced [23,34]:

$$\mathbf{T} = \begin{bmatrix} \text{Re}(\mathbf{V}_1) & \text{Im}(\mathbf{V}_1) & \text{Re}(\mathbf{V}_3) & \text{Im}(\mathbf{V}_3) & \text{Re}(\mathbf{V}_5) & \text{Im}(\mathbf{V}_5) \end{bmatrix}$$

The third step is to obtain the first-order Jordan form of Eq. (7) by changing the linear basis with the transform $\tilde{\mathbf{q}} = \mathbf{T}\mathbf{y}$. The dynamics for $\mathbf{y}$ thus writes

$$\mathbf{y}' = \mathbf{W}\mathbf{y} + \tilde{\mathbf{b}} \qquad (8)$$

where $\tilde{\mathbf{b}} = \mathbf{T}^{-1}\mathbf{b}$ and $\mathbf{W} = \mathbf{T}^{-1}\mathbf{A}\mathbf{T}$. It is reminded to the reader that in this expression, the elements of $\tilde{\mathbf{b}}$ are function of ξ_α, ξ_h, and ξ.

The fourth step is to reduce Eq. (8) to its first-order center manifold [34,35,38,39]. For a system encompassing only third-order nonlinearities, this corresponds to neglect variables not related to the bifurcation, i.e., y_3–y_6

$$\begin{bmatrix} y'_1 \\ y'_2 \end{bmatrix} = \begin{bmatrix} 0 & \omega_1 \\ -\omega_1 & 0 \end{bmatrix} \begin{bmatrix} y_1 \\ y_2 \end{bmatrix} + \begin{bmatrix} \tilde{b}_1 \\ \tilde{b}_2 \end{bmatrix} \qquad (9)$$

where $\tilde{b}_1$ and $\tilde{b}_2$ are the following polynomial functions:

$$\begin{aligned} \tilde{b}_1 &= c_{30}(\xi_\alpha, \xi_h, \xi)\,y_1^3 + c_{21}(\xi_\alpha, \xi_h, \xi)\,y_1^2 y_2 \\ &\quad + c_{12}(\xi_\alpha, \xi_h, \xi)\,y_1 y_2^2 + c_{03}(\xi_\alpha, \xi_h, \xi)\,y_2^3 \\ \tilde{b}_2 &= d_{30}(\xi_\alpha, \xi_h, \xi)\,y_1^3 + d_{21}(\xi_\alpha, \xi_h, \xi)\,y_1^2 y_2 \\ &\quad + d_{12}(\xi_\alpha, \xi_h, \xi)\,y_1 y_2^2 + d_{03}(\xi_\alpha, \xi_h, \xi)\,y_2^3 \end{aligned} \qquad (10)$$

The expression of the $c_{ij}(\xi_\alpha, \xi_h, \xi)$ and $d_{ij}(\xi_\alpha, \xi_h, \xi)$ coefficients are given in Appendix C.

The fifth step is to operate the following polar transformation:

$$y_1 = r\cos(\omega_1) \text{ and } y_2 = r\sin(\omega_1)$$

where $r \in \mathbb{R}$. Unfolding the singularity in the vicinity of the critical point [35,36], the Hopf bifurcation can be locally described with

$$r' = \lambda_\alpha\big(\tilde{U} - \tilde{U}_f\big)r + \rho r^3 \qquad (11)$$

where $\lambda_\alpha = \partial\lambda/\partial\tilde{U}$ and $\lambda = \lambda_1$ for any $\tilde{U}$; λ_α is estimated numerically. That is, λ_1 is calculated for a flow speed $\tilde{U}$ slightly larger than $\tilde{U}_f$ ($\sim 0.05\%$), and the slope between the two is calculated. It has to be noticed that Eq. (11) is only valid for $\tilde{U}$ in a neighborhood of $\tilde{U}_f$, because Eqs. (9)–(11) result from a local analysis at criticality. The validity of this neighborhood will be discussed in Sec. 4.2.1. Eventually, it can be proven [35] that

$$\rho = (1/8)(3c_{30} + c_{12} + d_{21} + 3d_{03}) \qquad (12)$$

The nontrivial solution of Eq. (11) is equal to $\sqrt{-\lambda_\alpha(\tilde{U} - \tilde{U}_f)/\rho}$. Thus, if $\rho > 0$, this solution is valid for $\tilde{U} < \tilde{U}_f$, and the bifurcation is subcritical. Otherwise, if $\rho < 0$, the nontrivial solution of Eq. (11) is valid for $\tilde{U} > \tilde{U}_f$, and the bifurcation is supercritical. The value of ξ for which $\rho = 0$ (denoted ξ_c) is a linear function of ξ_α and ξ_h and can directly be derived from Eq. (12). The expression of ξ_c is found by using the parameters from Tables 1 and 2 and yields

$$\xi_c = 0.0116\xi_h + 0.0966\xi_\alpha \qquad (13)$$

If $\xi > \xi_c$, the instability is supercritical, and if $\xi < \xi_c$, the instability is subcritical. The nonlinearity of the NLTVA is thus able to cancel the subcriticality of the bifurcation. The validation of the analytical procedure described above as well as the behavior of the system in the post-critical regime is investigated in Sec. 4.2.

4.2   Post-Critical Regime. The analytical procedure described above is compared with numerical solutions obtained by a continuation technique, using a pseudo-arclength method implemented in the software AUTO [40].

The post-critical regime is explored for a hard and a soft pitch spring, i.e., $\xi_\alpha > 0$ and $\xi_\alpha < 0$, respectively. A hard spring can be used to represent a thin wing or a propeller blade, whereas a soft spring may be associated with panel buckling [27,41]. Nonlinear restoring force is considered only on the pitch motions so that $\xi_h = 0$. This assumption is justified by the fact that in the post-critical regime, LCOs' amplitudes are very small on the plunge mode, so that the cubic nonlinearity is not excited. Moreover, it has been verified in all the numerical results presented that setting $\xi_h = 1$ does not change significantly the bifurcation behavior.

First, the hard pitch spring is investigated. This configuration is similar to the one studied by Lee et al. [27]. Second, the configuration with a soft pitch spring is explored. This case is similar to the one studied by Pettit and Beran [28]. In this case, a quintic stiffness is added to the pitch stiffness in order to have stable solutions in the post-critical regime.

4.2.1   Hard Pitch Spring. In a similar manner as in Ref. [27], we set here the nonlinear restoring forces to $\xi_\alpha = 1$ and $\xi_h = 0$.

The bifurcation diagram for the airfoil without absorber (i.e., with $\varepsilon = 0$) is first shown in Figs. 6(a) and 6(b). The result corresponds to a supercritical Hopf bifurcation. The analytical solution obtained in Sec. 4.1 is also represented, showing a very good agreement for small amplitude oscillations.

The case with an NLTVA without nonlinearities (i.e., $\xi = 0$), which is equivalent to a TMD, is shown in Figs. 6(c) and 6(d). As
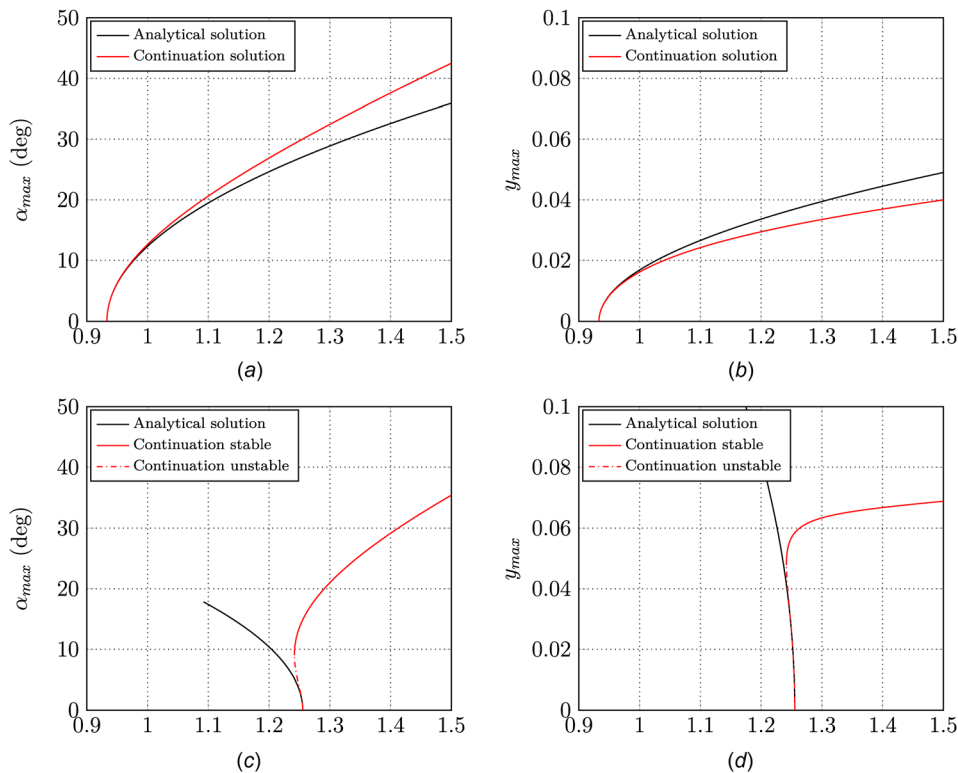
Fig. 6 Bifurcation diagram of pitch and plunge mode for the system without absorber (a) and (b) and in the presence of an NLTVA without nonlinearities (c) and (d)

predicted by the linear stability analysis, the flutter velocity is repelled from 0.93 to 1.26. Nevertheless, the Hopf bifurcation becomes subcritical. Hence, a detrimental effect of repelling the flutter velocity is to shift the originally supercritical Hopf bifurcation to a subcritical one. The most salient disadvantage of subcriticality lies in the appearance of a jump phenomenon at the flutter velocity, when increasing (and decreasing) the flow speed. In this example, when $\tilde{U}$ is slightly larger than $\tilde{U}_f$, the amplitude of pitch motion varies suddenly from 0 to 15 deg, which may cause serious damage to the structure. Another effect of the subcriticality is the existence of a bistable region for flow velocities smaller than the flutter velocity.

We now investigate the influence of the nonlinear stiffness ξ of the NLTVA on the Hopf bifurcation criticality. For that purpose, the bifurcation diagram is plotted for four increasing values of ξ in Fig. 7. The four selected cases are

(1) $\xi = 0.06$ ($\xi < \xi_c$), where the subcriticality is less pronounced than for $\xi = 0$;

(2) $\xi = 0.0966$ ($\xi = \xi_c$), where, according to the analytical prediction, there is a transition between subcritical and supercritical behavior;

(3) $\xi = 0.217$ ($\xi_c < \xi < \xi_s$, where $\xi_s = 0.218$), which is the largest value of ξ before a global bifurcation appearance; and

(4) $\xi = 0.218$ ($\xi = \xi_s$), where a global bifurcation suddenly occurs in the diagram, with appearance of two limit points, as well as two Neimarck–Sacker bifurcations points with in between quasiperiodic solutions.

These results clearly evidenced the effect of the NLTVA on the bifurcation diagram. Increasing the cubic stiffness ξ turns out to make the bifurcation more and more supercritical. However, the global behavior is also affected so that the optimal value is not the largest possible value of ξ. The global bifurcation occurring for $\xi_s = 0.218$ modifies drastically the diagram, which is then nonoptimal in a design point of view. Indeed, the two limit points give rise to a new global subcritical behavior with the appearance of a solution branch with large amplitude that persists for smaller
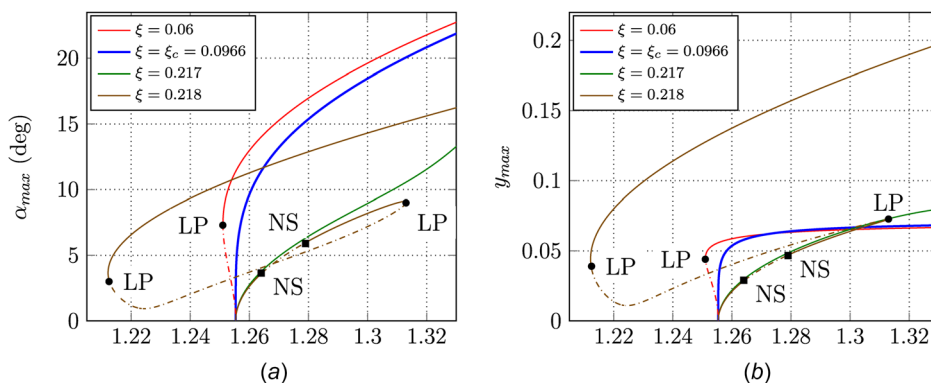
Fig. 7 Bifurcation diagram of (a) pitch and (b) plunge mode for four increasing values of ξ. The solid lines correspond to the stable solutions and the dashed line to the unstable ones. LP stands for limit point and NS for Neimark–Sacker bifurcation point.
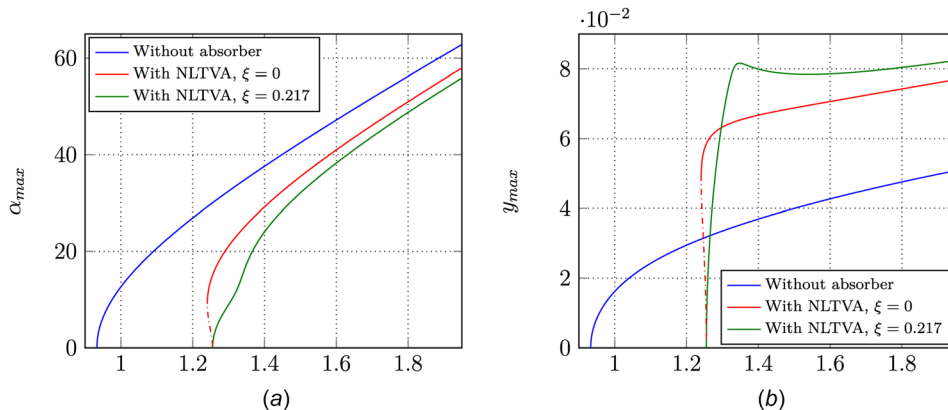
**Fig. 8 Influence of the NLTVA with $\xi = 0$ and $\xi = 0.217$ on the bifurcation diagram of the 2dofs airfoil**

values of $\tilde{U}_f$. Hence, this situation is to be avoided, and optimal values for ξ are founded with $\xi > \xi_c$ (ensuring supercriticality) and $\xi < \xi_s$ (avoiding an extra global bifurcation scenario); the largest decrease of LCO amplitude on pitch being obtained with $\xi = 0.217$. This case could be optimal, but its robustness is not satisfactory since $\xi = 0.218$ gives a detrimental global bifurcation scenario. Furthermore, the abrupt and drastic transition of the scenario for ξ varying from $\xi = 0.217$ to $\xi = 0.218$ suggests that periodic stable solutions probably exist also for $\xi < 0.218$ and $\tilde{U} < \tilde{U}_f$. However, a detailed analysis of this aspect is out of the scope of this study.

The influence of the NLTVA is summarized in Fig. 8. The LCO amplitude on pitch has been reduced significantly by the NLTVA. For example, at $\tilde{U} = 1.4$, the LCO amplitude on pitch has been decreased by 36.4% compared to the case without absorber. Nevertheless, at the same time, the LCO amplitude on plunge has been increased by 115.9%. Even if this increase seems large, it is remarked that the more inconvenient LCO are those on

the pitch mode, because this is the most energetic mode of the system in the post-critical regime and even after an increase of 115.9% the LCO amplitude on plunge remains very small (8% of the semichord).

In order to study the influence of the NLTVA on the 2dofs airfoil transient regime, direct numerical simulations of the system Eq. (2) without absorber and with an NLTVA tuned as $\xi = 0.217$ are conducted and plotted in Fig. 9. The time integration is realized using a fourth-order Runge–Kutta scheme.

A first set of simulations, Figs. 9(a)–9(c), is realized for $\tilde{U} = 1.1$. This flow velocity is beyond the flutter velocity, $\tilde{U}_f^{\text{noTVA}}$, of the system without absorber but below the flutter velocity, $\tilde{U}_f^{\text{NLTVA}}$, of the system with the NLTVA. The initial conditions are set to zero except for the initial amplitude of the pitch mode, which is set equal to $\alpha(0) = 10$ deg. The initial pitch amplitude has been chosen large in order to have a long transient regime. As predicted by the continuation procedure, without absorber, the
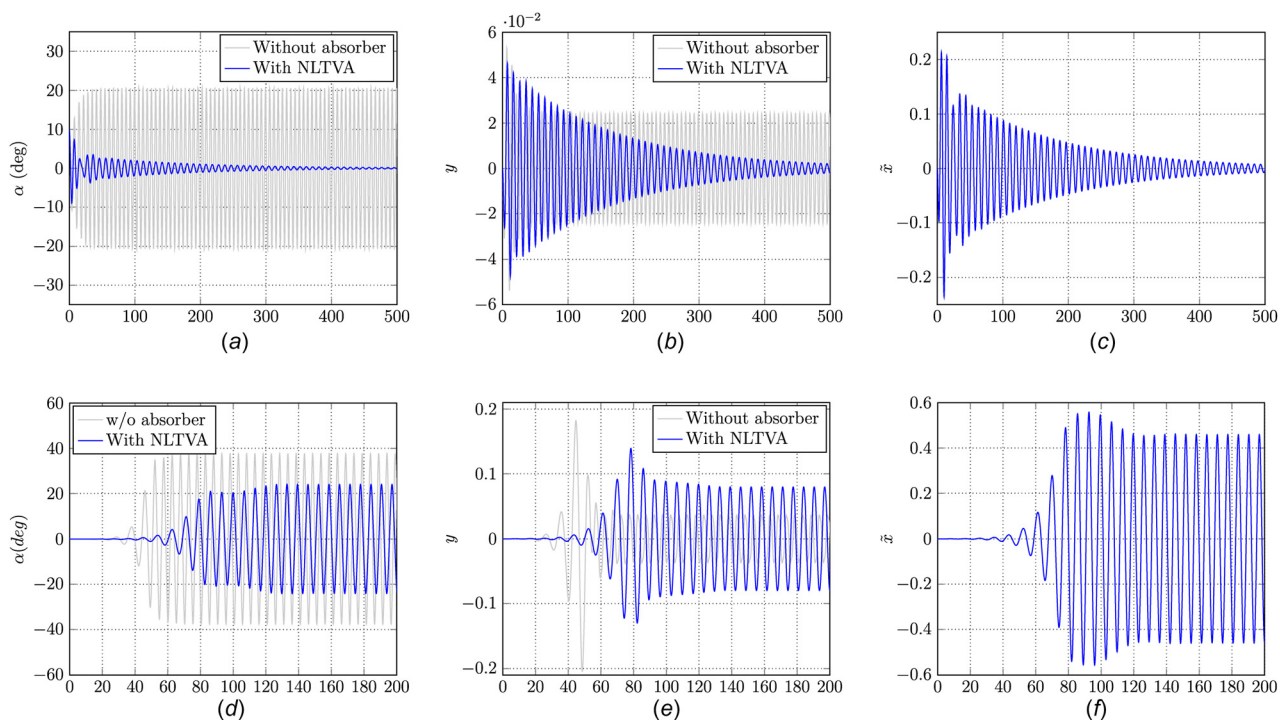
Fig. 9 Time series simulations corresponding to Fig. 8 with and without absorber at $\tilde{U} = 1.1$ (a)–(c) and $\tilde{U} = 1.4$ (d)–(f). The NLTVA is set such as $\xi = 0.217$. The initial conditions are equal to zero except for the initial amplitude of the pitch mode, which is set equal to $\alpha(0) = 10$ deg for (a)–(c) and to $\alpha(0) = 6.10^{-3}$ deg for (d)–(f).

transient regime leads to limit cycles of amplitude 20 deg on pitch and 0.024 on plunge; while, with the NLTVA, the oscillations are canceled. Moreover, the NLTVA has the largest damping effect on the pitch transient response. Indeed, as shown in Fig. 8, the NLTVA reduces the oscillations amplitude on pitch but increases those on plunge.

A second set of simulations, Figs. 9(d)–9(f), is realized for $\tilde{U} = 1.4$. This flow velocity is beyond $\tilde{U}_f^{\text{noTVA}}$ and $\tilde{U}_f^{\text{NLTVA}}$. The initial conditions are set to zero except for the initial amplitude of the pitch mode, which is set equal to $\alpha(0) = 6.10^{-3}$ deg. Because the flow velocity is beyond $\tilde{U}_f^{\text{noTVA}}$ and $\tilde{U}_f^{\text{NLTVA}}$, the transient regimes with and without NLTVA lead to limit cycles. Furthermore, the NLTVA postpones the limit cycle apparition, the LCOs settle down around $\tau \simeq 73$ without the absorber and around $\tau \simeq 139$ with the NLTVA. Indeed, when the flow speed is close to the flutter velocity, the growth rate is small and the transient regime is long. Thus, the transient regime is longer for the system with NLTVA.

4.2.2 Soft Pitch Spring. In this section, the influence of the NLTVA on the airfoil with a soft pitch spring is investigated. That is $\xi_\alpha = -1$ and $\xi_h = 0$. Moreover, a quintic stiffness, named $\xi_{\alpha 5}$, is added to the pitch restoring force, which means that the vector **b** from Eq. (7) becomes

$$\mathbf{b} = \begin{bmatrix} 0 \\ 0 \\ 0 \\ -\mathbf{M}^{-1} \begin{bmatrix} \xi_h y^3 + \varepsilon\xi(y - \tilde{x} - \lambda\alpha)^3 \\ \xi_\alpha \alpha^3 + \xi_{\alpha 5}\alpha^5 + \varepsilon\xi\lambda(\tilde{x} - y + \lambda\alpha)^3 \\ \xi(\tilde{x} - y + \lambda\alpha)^3 \end{bmatrix} \end{bmatrix}$$

We choose in this study $\xi_{\alpha 5} = 7$, this configuration is similar to the case studied by Pettit and Beran [28].

As Sec. 4.2.1, the effect of ξ on the airfoil bifurcation diagram is investigated. For that purpose, the bifurcation diagram is computed for five increasing values of ξ from -0.5 to 0.4, and the results are shown in Fig. 9. The key values are the following:

- $\xi_c = -0.0966$, which is the critical value predicted from the analytical study using Eq. (13). When $\xi \geq \xi_c$, the bifurcation is supercritical, otherwise it is subcritical.
- $\xi_{s_1} = -0.15$ and $\xi_{s_2} = 0.125$: between these two values, a global bifurcation occurs and the solution branches encounters Neimark–Sacker bifurcations, resulting in a more complex shape of the diagram.
- $\xi = 0$ which corresponds to the TMD.

Around the criticality, detailed in Figs. 10(c) and 10(d), the effect of increasing ξ is to bend the bifurcation branch to the right. In order to have a supercritical behavior, one would have thus expect that selecting a larger value than $\xi_c = -0.0966$ could have been sufficient. However, the numerical simulation shows that ensuring supercriticality with $\xi \geq \xi_c$ in the vicinity of the critical flutter velocity do not avoid the occurrence of a global subcritical behavior. Increasing ξ worsens the scenario with a large amplitude branch going down to smaller velocities, even though locally the supercriticality is enforced. In particular, the cases $\xi = \xi_c = -0.0966$ and $\xi = 0$ shown in Figs. 10(a) and 10(b) show large amplitudes especially present in the plunge mode, which are not acceptable in a design perspective to mitigate the flutter instability. And still increasing ξ is definitely not a solution, as the situation worsens as soon as $\xi > \xi_{s_2}$, as exemplified with the case $\xi = 0.4$.
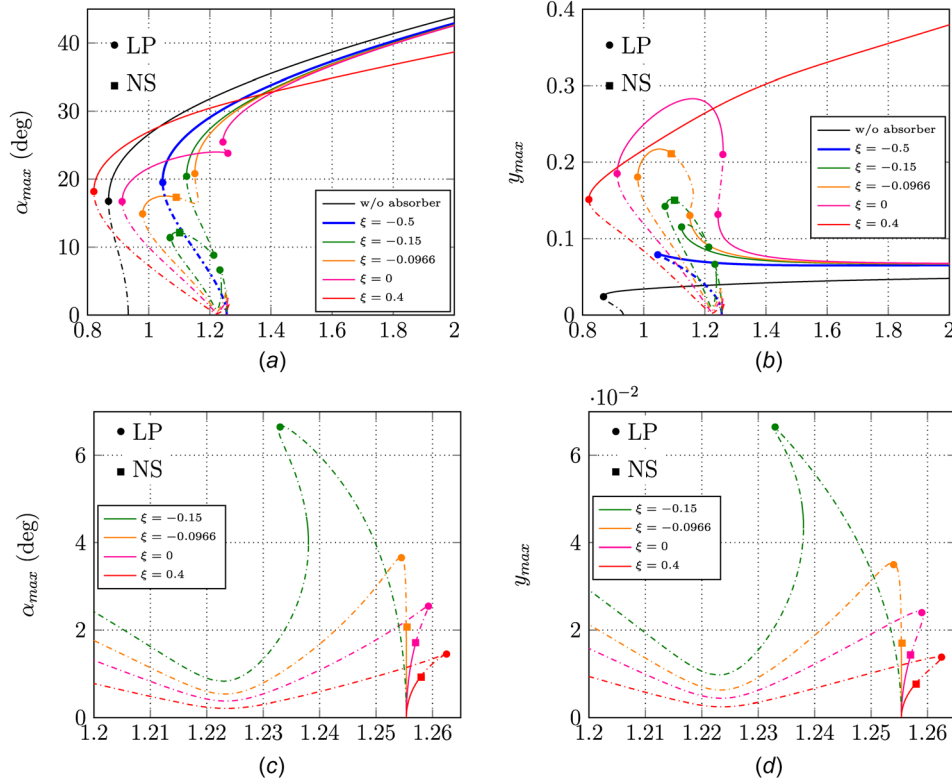
Fig. 10 Bifurcation diagram of (a) and (c) pitch and (b) and (d) plunge mode for increasing values of ξ. The solid lines correspond to the stable solutions and the dashed line to the unstable ones. The plots (c) and (d) detail the bifurcation diagram around the criticality for $\xi \geq -0.15$. LP stands for limit point and NS for Neimark–Sacker bifurcation point.

In this more difficult case, a compromise must be found between the acceptable subcriticality and the amplitudes of LCOs in the post-critical regime. With this aim in view, the case $\xi = -0.5$ shown in Fig. 9 could represent such an optimal, with a small interval of subcriticality together with reduced amplitude of the LCOs. Depending on the context and the design constraints, $\xi = -0.15$ also represents an interesting case for the control of the flutter instability. Nevertheless the softening spring case is more difficult to handle than the precedent hardening spring case, and an optimal control as initially desired is out of reach with the present NLTVA design.

5 Conclusion

The influence of an NLTVA on the airfoil flutter instability has been investigated. The NLTVA is defined by two parameters: its linear stiffness, which can be tuned in order to repel as much as possible the flutter velocity U_f; and its nonlinear stiffness, which can be used for a better control of the bifurcation diagram. Linear stability analysis has shown that the flutter velocity can indeed be repelled by finding optimal values of stiffness together with the damping ratio of the absorber. Important gains ranging roughly from 30% to more than 150% can be theoretically achieved. A design rule has also been provided by means of a polynomial fit of the optimal parameters, for varying values defining the studied airfoil.

A nonlinear analysis has then been conducted, including a local analytical prediction, and a bifurcation study for a hardening and a softening pitch spring stiffness. The results show that in the hardening case, an optimal tuning is achieved, controlling the bifurcation in a supercritical case with an important gain in the LCOs amplitudes. The softening case has been found more difficult to optimize, and a compromise between subcriticality and large amplitude LCOs has to be found, depending on the context.

Acknowledgment

Appendix A: Coefficients of Eq. (5)

$$a_6 = r_\alpha^2 - x_\alpha^2 \quad a_5 = \left(\zeta_h + (1+\varepsilon)\zeta\right)r_\alpha^2 + \left(\nu x_\alpha + b r_\alpha^2\right)\tilde{U}$$
$$+ \zeta_\alpha - x_\alpha^2 \zeta + (2x_\alpha + \lambda)\varepsilon\lambda\zeta$$

$$a_4 = \left(\Omega^2 + \zeta\zeta_h + (1+\varepsilon)\gamma + 1\right)r_\alpha^2 + \left(\beta\zeta_\alpha + \left(\nu x_\alpha + r_\alpha^2\beta\right)\zeta\right)\tilde{U}$$
$$- (\beta x_\alpha + \nu)\tilde{U}^2 + \left(\zeta_h + (1+\varepsilon)\zeta\right)\zeta_\alpha + \varepsilon\lambda^2\zeta\zeta_h$$
$$- \gamma x_\alpha^2 + (2x_\alpha + \lambda)\varepsilon\gamma\lambda$$

$$a_3 = \left(\zeta\Omega^2 + (1+\gamma)\zeta_h\right.$$
$$+ (1+\varepsilon)\zeta)r_\alpha^2 - \left(\nu\zeta_h + \beta x_\alpha\zeta + (1+\varepsilon)\nu\zeta\right)\tilde{U}^2$$
$$+ \left(\beta\zeta\zeta_\alpha + \gamma\nu x_\alpha + r_\alpha^2\beta(1+\gamma)\right)\tilde{U} + \left(\zeta\zeta_\alpha + \varepsilon\gamma\lambda^2\right)\zeta_h$$
$$+ (1+\varepsilon)\gamma\zeta_\alpha + \left(\zeta_\alpha + \varepsilon\lambda^2\zeta\right)\Omega^2$$

$$a_2 = \left((1+\gamma)\Omega^2 + \zeta\zeta_h + (1+\varepsilon)\gamma\right)r_\alpha^2$$
$$- \left(\nu\Omega^2 + \nu\zeta\zeta_h + \beta\gamma x_\alpha + (1+\varepsilon)\gamma\nu\right)\tilde{U}^2$$
$$+ \beta\left(\gamma\zeta_\alpha + r_\alpha^2\zeta\right)\tilde{U} + \left(\zeta\zeta_\alpha + \varepsilon\gamma\lambda^2\right)\Omega^2 + \gamma\zeta_\alpha\zeta_h$$

$$a_1 = \left(\zeta\Omega^2 + \gamma\zeta_h\right)r_\alpha^2 - \nu\left(\zeta\Omega^2 + \gamma\zeta_h\right)\tilde{U}^2 + \beta\gamma r_\alpha^2\tilde{U}$$
$$+ \gamma\zeta_\alpha\Omega^2 a_0 = \left(r_\alpha^2 - \nu\tilde{U}^2\right)\gamma\Omega^2$$

Appendix B: Coefficients of Eq. (6)

The majority of the coefficients a_{ijk} and b_{ijk} from Eq. (6) are neglectable. The non-neglectable coefficients a_{ijk} and b_{ijk} are

$a_{000} = 0.328$	$a_{100} = -0.629$	$a_{200} = 0.173$	$a_{300} = 0.294$
$a_{010} = 0.604$	$a_{210} = 0.165$	$a_{030} = -0.124$	$a_{001} = 0.486$
$a_{101} = -0.437$	$a_{111} = -0.113$	$a_{021} = -0.275$	$a_{002} = 0.278$
$a_{102} = -0.254$	$a_{003} = 0.142$	$a_{103} = -0.143$	
$b_{000} = 0.11$	$b_{100} = 0.0475$	$b_{200} = -0.0701$	$b_{300} = -0.174$
$b_{010} = 0.00307$	$b_{210} = 0.174$	$b_{030} = -0.0329$	$b_{001} = -0.00415$
$b_{101} = -0.128$	$b_{111} = 0.106$	$b_{021} = 0.0164$	$b_{002} = -0.081$
$b_{102} = -0.0444$	$b_{003} = -0.00191$	$b_{103} = 0.00259$	

Appendix C: Coefficients of Eq. (10)

The nonlinear coefficients of the cubic polynomial terms appearing in Eq. (10) are here detailed. Since the first transformation matrix has no simple analytic expression, the numerical values of the coefficients are given, which correspond to the airfoil parameters of the reference case given in Table 1 and to the optimal NLTVA linear parameters given in Table 2.

$c_{30} = 0.047\,\xi_h - 0.064\,\xi_\alpha - 4.9\,\xi$	$d_{30} = -0.01\,\xi_h - 0.43\,\xi_\alpha - 0.28\,\xi$
$c_{21} = -0.054\,\xi_h + 0.16\,\xi_\alpha + 2.6\,\xi$	$d_{21} = 0.012\,\xi_h + 1.1\,\xi_\alpha + 0.15\,\xi$
$c_{12} = 0.021\,\xi_h - 0.13\,\xi_\alpha - 0.46\,\xi$	$d_{12} = -4.5.10^{-3}\,\xi_h - 0.87\,\xi_\alpha - 0.026\,\xi$
$c_{03} = -2.7.10^{-3}\,\xi_h + 0.036\,\xi_\alpha$	$d_{03} = 5.7.10^{-4}\,\xi_h + 0.24\,\xi_\alpha + 1.5.10^{-3}\,\xi$
$\qquad + 0.027\,\xi$	

References

[1] Vipperman, J. S., Clark, R. L., Conner, M., and Dowell, E. H., 1998, "Experimental Active Control of a Typical Section Using a Trailing-Edge Flap," J. Aircr., 35(2), pp. 224–229.

[2] Karpel, M., 1982, "Design for Active Flutter Suppression and Gust Alleviation Using State-Space Aeroelastic Modeling," J. Aircr., 19(3), pp. 221–227.

[3] Ko, J., Kurdila, A. J., and Strganac, T. W., 1997, "Nonlinear Control of a Prototypical Wing Section With Torsional Nonlinearity," J. Guid., Control, Dyn., 20(6), pp. 1181–1189.

[4] Heeg, J., 1993, "Analytical and Experimental Investigation of Flutter Suppression by Piezoelectric Actuation," NASA Langley Research Center, Hampton, VA, Technical Report No. NASA-TP-3241.

[5] Dowell, E. H., 2004, A Modern Course in Aeroelasticity, Kluwer Academic Publishers, Boston, MA.

[6] Malher, A., Doaré, O., and Touzé, C., 2017, "Influence of a Hysteretic Damper on the Flutter Instability," J. Fluids Struct., 68, pp. 356–369.

[7] Kwon, S.-D., and Park, K.-S., 2004, "Suppression of Bridge Flutter Using Tuned Mass Dampers Based on Robust Performance Design," J. Wind Eng. Ind. Aerodyn., 92(11), pp. 919–934.

[8] Vaurigaud, B., Manevitch, L. I., and Lamarque, C.-H., 2011, "Passive Control of Aeroelastic Instability in a Long Span Bridge Model Prone to Coupled Flutter Using Targeted Energy Transfer," J. Sound Vib., 330(11), pp. 2580–2595.

[9] Pourzeynali, S., and Datta, T., 2002, "Control of Flutter of Suspension Bridge Deck Using TMD," Wind Struct., 5(5), pp. 407–422.

[10] Den Hartog, J. P., 1934, Mechanical Vibrations, McGraw-Hill Book Company, New York.

[11] Gattulli, V., Di Fabio, F., and Luongo, A., 2004, "Nonlinear Tuned Mass Damper for Self-Excited Oscillations," Wind Struct., 7(4), pp. 251–264.

[12] Lee, Y. S., Vakakis, A., Bergman, L., McFarland, D. M., and Kerschen, G., 2007, "Suppressing Aeroelastic Instability Using Broadband Passive Targeted Energy Transfers, Part 1: Theory," AIAA J., 45(3), pp. 693–711.

[13] Lee, Y. S., Kerschen, G., McFarland, D. M., Hill, W. J., Nichkawde, C., Strganac, T. W., Bergman, L. A., and Vakakis, A. F., 2007, "Suppressing Aeroelastic Instability Using Broadband Passive Targeted Energy Transfers—Part 2: Experiments," AIAA J., 45(10), pp. 2391–2400.

[14] Gendelman, O. V., 2001, "Transition of Energy to a Nonlinear Localized Mode in a Highly Asymmetric System of Two Oscillators," Nonlinear Dyn., 25(1–3), pp. 237–253.

[15] Vakakis, A. F., and Gendelman, O., 2001, "Energy Pumping in Nonlinear Mechanical Oscillators—Part II: Resonance Capture," ASME J. Appl. Mech., 68(1), pp. 42–48.

[16] Vakakis, A. F., Manevitch, L. I., Gendelman, O., and Bergman, L., 2003, "Dynamics of Linear Discrete Systems Connected to Local, Essentially Non-Linear Attachments," J. Sound Vib., 264(3), pp. 559–577.

[17] Vakakis, A. F., Gendelman, O. V., Bergman, L. A., McFarland, D. M., Kerschen, G., and Lee, Y. S., 2008, *Nonlinear Targeted Energy Transfer in Mechanical and Structural Systems*, Vol. 156. Springer, New York.

[18] Gendelman, O. V., Vakakis, A. F., Bergman, L. A., and McFarland, D. M., 2010, "Asymptotic Analysis of Passive Nonlinear Suppression of Aeroelastic Instabilities of a Rigid Wing in Subsonic Flow," SIAM J. Appl. Math., **70**(5), pp. 1655–1677.

[19] Hubbard, S. A., Fontenot, R. L., McFarland, D. M., Cizmas, P. G., Bergman, L. A., Strganac, T. W., and Vakakis, A. F., 2014, "Transonic Aeroelastic Instability Suppression for a Swept Wing by Targeted Energy Transfer," J. Aircr., **51**(5), pp. 1467–1482.

[20] Viguié, R., and Kerschen, G., 2009, "Nonlinear Vibration Absorber Coupled to a Nonlinear Primary System: A Tuning Methodology," J. Sound Vib., **326**(3), pp. 780–793.

[21] Habib, G., Detroux, T., Viguié, R., and Kerschen, G., 2015, "Nonlinear Generalization of Den Hartog's Equal-Peak Method," Mech. Syst. Signal Process., **52–53**, pp. 17–28.

[22] Habib, G., and Kerschen, G., 2016, "A Principle of Similarity for Nonlinear Vibration Absorbers," Physica D: Nonlinear Phenom., **332**(1), pp. 1–8.

[23] Habib, G., and Kerschen, G., 2015, "Suppression of Limit Cycle Oscillations Using the Nonlinear Tuned Vibration Absorber," Proc. R. Soc. London, **471**(2176), p. 20140976.

[24] Grappasonni, C., Habib, G., Detroux, T., and Kerschen, G., 2016, "Experimental Demonstration of a 3D-Printed Nonlinear Tuned Vibration Absorber," *Nonlinear Dynamics* (Conference Proceedings of the Society for Experimental Mechanics Series), Vol. 1, Springer, Cham, Switzerland, pp. 173–183.

[25] Benacchio, S., Malher, A., Boisson, J., and Touzé, C., 2016, "Design of a Magnetic Vibration Absorber With Tunable Stiffnesses," Nonlinear Dyn., **85**(2), pp. 893–911.

[26] Lacarbonara, W., and Cetraro, M., 2011, "Flutter Control of a Lifting Surface Via Visco-Hysteretic Vibration Absorbers," Int. J. Aeronaut. Space Sci., **12**(4), pp. 331–345.

[27] Lee, B. H. K., Jiang, L., and Wong, Y., 1998, "Flutter of an Airfoil With a Cubic Nonlinear Restoring Force," AIAA Paper No. AIAA-98-1725

[28] Pettit, C. L., and Beran, P. S., 2003, "Effects of Parametric Uncertainty on Airfoil Limit Cycle Oscillation," J. Aircr., **40**(5), pp. 1004–1006.

[29] Bisplinghoff, R. L., and Ashley, H., 1962, *Principles of Aeroelasticity*, Wiley, New York.

[30] Fung, Y. C., 2002, *An Introduction to the Theory of Aeroelasticity*, Dover Publications, Mineola, NY.

[31] Lee, Y. S., Vakakis, A. F., Bergman, L. A., McFarland, D. M., and Kerschen, G., 2005, "Triggering Mechansms of Limit Cycle Oscillations Due to Aeroelastic Instability," J. Fluids Struct., **21**(5–7), pp. 485–529.

[32] Amandolèse, X., Michelin, S., and Choquel, M., 2013, "Low Speed Flutter and Limit Cycle Oscillations of a Two-Degree-of-Freedom Flat Plate in a Wind Tunnel," J. Fluids Struct., **43**, pp. 244–255.

[33] Dimitriadis, G., and Li, J., 2009, "Bifurcation Behavior of Airfoil Undergoing Stall Flutter Oscillations in Low-Speed Wind Tunnel," AIAA J., **47**(11), pp. 2577–2596.

[34] Kuznetsov, Y. A., 2013, *Elements of Applied Bifurcation Theory*, Vol. 112, Springer, New York.

[35] Guckenheimer, J., and Holmes, P., 2013, *Nonlinear Oscillations, Dynamical Systems, and Bifurcations of Vector Fields*, Springer, New York.

[36] Manneville, P., 1995, "Dissipative Structures and Weak Turbulence," *Chaos—The Interplay Between Stochastic and Deterministic Behaviour*, Springer, New York, pp. 257–272.

[37] Iooss, G., and Adelmeyer, M., 1998, *Topics in Bifurcation Theory and Applications*, World Scientific, Singapore.

[38] Gai, G., and Timme, S., 2016, "Nonlinear Reduced-Order Modelling for Limit-Cycle Oscillation Analysis," Nonlinear Dyn., **84**(2), pp. 991–1009.

[39] Touzé, C., Thomas, O., and Chaigne, A., 2004, "Hardening/Softening Behaviour in Non-Linear Oscillations of Structural Systems Using Non-Linear Normal Modes," J. Sound Vib., **273**(1), pp. 77–101.

[40] Doedel, E. J., Paffenroth, R. C., Champneys, A. R., Fairgrieve, T. F., Kuznetsov, Y. A., Sandstede, B., and Wang, X., 2002, "Auto 2000: Continuation and Bifurcation Software for Ordinary Differential Equations," Concordia University, Montreal, QC, Canada, Technical Report.

[41] Woolston, D. S., Runyan, H. L., and Andrews, R. E., 1957, "An Investigation of Effects of Certain Types of Structural Nonlinearities on Wing and Control Surface Flutter," J. Aeronaut. Sci., **24**(1), pp. 57–63.